Lyapunov Guidance Vector Fields for Unmanned Aircraft Applications

Eric W. Frew, *Member, IEEE,* Dale A. Lawrence, Cory Dixon, Jack Elston, and William J. Pisano

***Abstract*—This paper presents results implementing Lyapunov vector fields for the guidance of unmanned aircraft. The vector fields yield globally stable tracking of circular loiter patterns. These loiter patterns are used in several unmanned aircraft applications including hierarchical micro air vehicle control for cooperative plume tracking, extremum seeking for electronic chaining, and cooperative tracking of moving targets. Extensions of the basic LGVF approach are made for each application including: warping the circular pattern to form other closed orbit patterns; driving the center of the LGVF orbit using virtual dynamics; and spacing multiple unmanned aircraft around a circular orbit. Hardware-in-the-loop simulation results and flight data are given to validate performance.**

I. Introduction

THE Lyapunov vector field approach to unmanned aircraft guidance provides globally stable convergence to limit cycle behavior about closed loiter patterns [1,2] and enables decomposition of cooperative tasks into a hierarchical architecture that exhibits complex behavior through the interaction of simple, provably stable, layers. Compared to most unmanned ground vehicles and unmanned helicopters, fixed wing aircraft must maintain significant forward flight speed in order to remain aloft and have a minimum possible turning radius. These constraints complicate the design of automated planning systems for unmanned aircraft systems (UAS) and typically lead to complex nonlinear algorithms. Using the Lyapunov guidance vector field (LGVF) as the low level guidance layer, higher layers in the control architecture only need to consider the dynamics of the loiter pattern center and can impose simple "virtual" dynamics on this point, including the ability to stop at a single location.

This paper describes three control systems for three different applications that take advantage of the hierarchical approach enabled by the LGVF concept. These applications include cooperative control of a flock of micro air vehicles tracking a chemical plume released in the atmosphere [3]; controlled mobility in an airborne communication network using distributed extremum seeking to mitigate noise and interference and to improve end-to-end throughput from source to destination over multiple hops [4]; and cooperative stand-off line-of-sight (CSLOS) tracking of moving targets for improved sensor coverage [1,2,5]. Extensions of the basic LGVF approach are made for each application and results are given to validate performance.

Eric W. Frew is an Assistant Professor in the Aerospace Engineering Sciences (AES) Department at the University of Colorado, Boulder. (eric.frew@colorado.edu).

Dale A. Lawrence is an Associate Professor in the AES Department at the University of Colorado, Boulder. (dale.lawrence@colorado.edu).

Cory Dixon is a PhD candidate in the AES Department at the University of Colorado, Boulder. (cory.dixon@colorado.edu).

Jack Elston is a PhD candidate in the AES Department at the University of Colorado, Boulder. (jack.elston@colorado.edu).

William J. Pisano is a PhD candidate in the AES Department at the University of Colorado, Boulder. (william.pisano@colorado.edu)

II. Lyapunov Guidance Vector Fields

The algorithms presented here assume the unmanned aircraft are equipped with a low-level control system that presents a kinematic model to the guidance layer. When expressed relative to a moving point $\mathbf{p}_t = [x_t, y_t]^T \in \Re^2$ with inertial speed $[\dot{x}_t, \dot{y}_t]^T \in \Re^2$, the aircraft model is

$$\begin{aligned} \dot{x}_r &= u_1 \cdot \cos\psi + W_x - \dot{x}_t \\ \dot{y}_r &= u_1 \cdot \sin\psi + W_y - \dot{y}_t \\ \dot{\psi} &= u_2 \end{aligned} \tag{1}$$

where $\mathbf{p} = [x, y]^T \in \Re^2$ is the two-dimensional inertial position of the aircraft, $\mathbf{p}_r = \mathbf{p} - \mathbf{p}_t = [x_r, y_r]^T \in \Re^2$ is the position of the aircraft relative to the target, $\psi \in [0, 2\pi)$ is the aircraft yaw angle (Fig. 1), $[W_x, W_y]^T \in \Re^2$ are the components of the background (horizontal) wind velocity, $0 < v_{\min} \le u_1 \le v_{\max}$ is the commanded airspeed and $|u_2| \le \omega_{\max}$ is the commanded turning rate. Aircraft guidance is determined by calculating the desired velocity from a Lyapunov vector field. Consider the Lyapunov function $V(\mathbf{p}_r) = \left(r^2 - r_d^2\right)^2$, where $r^2 = \mathbf{p}_r^T \mathbf{p}_r$ is the squared radial distance of the UA from the loiter center. The total time derivative of $V(\mathbf{p}_r)$ can be specified to be non-positive by choosing desired relative vehicle velocity according to the guidance vector field

$$\mathbf{f}(\mathbf{p}_r) = \begin{bmatrix} \dot{x}_d \\ \dot{y}_d \end{bmatrix} = \frac{-\alpha v_0}{r\left(r^2 + r_d^2\right)} \cdot \begin{bmatrix} x_r \cdot \left(r^2 - r_d^2\right) + y_r \cdot 2rr_d \\ y_r \cdot \left(r^2 - r_d^2\right) - x_r \cdot 2rr_d \end{bmatrix} \tag{2}$$

where α is non-negative. This vector field produces the non-positive rate of change of V

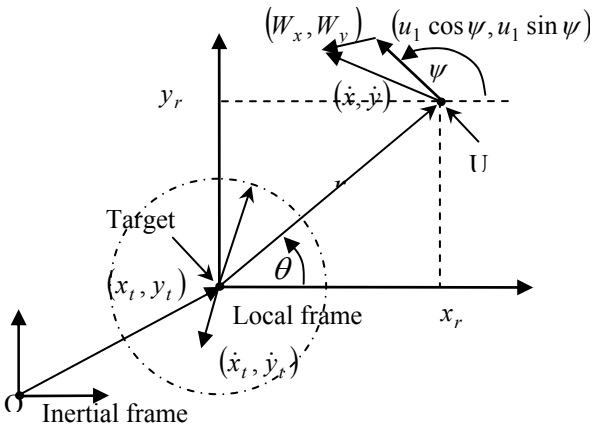

Fig. 1. Tracking geometry with the ground target of interest at the origin of the *local frame*.

$$\frac{dV}{dt} = \frac{-4\alpha v_o r\left(r^2 - r_d^2\right)^2}{r^2 + r_d^2}. \tag{3}$$

If α is bounded away from zero, $\dot{V}$ is zero and invariant only on the loiter circle $(r = r_d)$, ensuring [1,2] that the vector field produces a globally attractive limit cycle.

When the target and wind velocities are known, we take advantage of the variable scaling factor α in the Lyapunov vector field to recover the commanded air speed and retain global convergence [1,2]. Calculating the magnitude of the desired velocity of the UA relative to the background wind and setting it to the commanded air speed v_o leads to the following expression for the scale factor:

$$\begin{aligned}\alpha^2 \cdot \left(\dot{x}_d^2 + \dot{y}_d^2\right) + \alpha \cdot 2 \cdot \left(\dot{x}_d \cdot T_x + \dot{y}_d \cdot T_y\right) \\ + \left(T_x^2 + T_y^2\right) - v_0^2 = 0\end{aligned}. \tag{4}$$

where $\mathbf{T}=[T_x, T_y] = [\dot{x}_t - W_x, \dot{y}_t - W_y]$. Provided the UA speed v_0 is larger than the virtual target speed **T**, Eq. (4) has one positive real solution for α which preserves the aircraft air speed and maintains stability of the vector field.

The vector field gives the desired velocity which is used to generate the turn rate command

$$u_2 = \dot{\psi}_d - \lambda \cdot \left(\psi - \psi_d\right). \tag{5}$$

where ψ_d is the desired yaw angle

$$\psi_d = \arctan\left(\frac{\dot{y}_d + T_y}{\dot{x}_d + T_x}\right). \tag{6}$$

This commanded turn rate drives the heading angle error to zero which in turn puts the UA on the vector field that results in the desired loiter pattern. Figure 2 shows example data from the flight of a single micro air vehicle using the LGFV control approach.

III. Hierarchical MAV Control

Teams of cooperating micro air vehicles can efficiently perform *in situ* atmospheric sensing. In particular, toxic plume tracking in urban environments is challenging due to complex dispersion patterns created by large buildings and the high accuracy needed to direct mitigation efforts in areas with high population density.

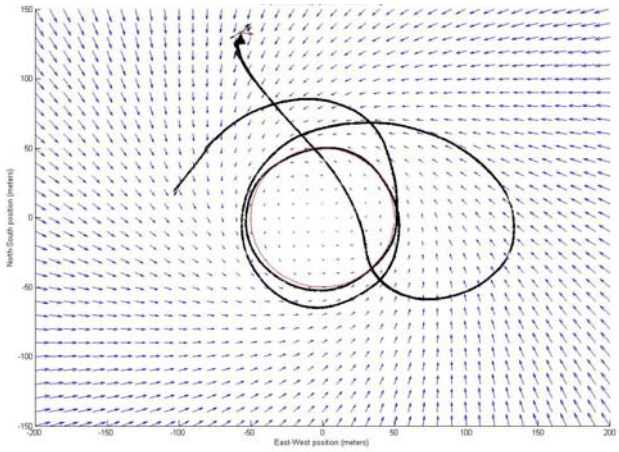

Fig. 2. Flight data using LGVF approach to control a micro air vehicle: autonomous take-off, loiter about a stationary target, land.

A hierarchical control architecture has been developed to enable cooperative tracking of toxic plumes by micro air vehicles. The control architecture contains four tiers each consisting of simple algorithms that lead to complex team behavior [3]. The lowest tier performs high rate propulsion and attitude control to maintain steady flight and individual guidance using the Lyapunov vector fields. The second tier uses potential field methods to direct the centers of the tier-one loiter circles. Tier three uses a hybrid system approach to assign MAVs to different behaviors corresponding to different tasks. Finally, tier four includes interaction with a human operator to interpret data and issues group commands.

The LGVF method is used as the basis of different low-level behaviors. A variety of alternative attractors can be obtained by a homeomorphic transformation of the basic circular loiter. This has the advantage of preserving the global stability properties of the vector field, but has some subtleties that can have unintended consequences. We consider approaches to produce a "racetrack" loiter pattern, which has applications in convoy protection [2] and airstrip approach and landing patterns.

Perhaps the simplest approach is to stretch (and possibly rotate) the circular vector field along one direction by using a simple change of coordinates (u,v) = h(x.y): e.g.

$$u = (1/k)x\,;\, v = y \tag{7}$$

The physical coordinates (x,y) produce warped coordinates (u,v) which are applied to the basic Lyapunov vector field Eq. (2) in place of (x,y), respectively. This produces a vector field $(\dot{u}, \dot{v})$ which is then unwarped via $(\dot{x}, \dot{y}) = h^{-1}(\dot{u}, \dot{v})$:

$$\dot{x} = k\dot{u} \; ; \; \dot{y} = \dot{v} \tag{8}$$

This produces an elliptical loiter circle, but it also distorts the vector directions so that contraction to the loiter ellipse is weaker in some regions than in others. As a result, loiter pattern tracking accuracy in the presence of disturbances may be poor along some portions of the pattern. Variations in the unwarping transformation can restore the tracking accuracy [10].

Instead of an ellipse, a racetrack pattern with straight sides can be obtained with a nonlinear change of coordinates.

$$u = \left(\frac{x}{k} * \frac{|x| + a}{|x| + b} \right)^2 \qquad a = \frac{R_d}{100} \quad b = (k-1) * R_d \tag{9}$$

where R_d is the desired radius (or one half the width) of the racetrack and k is the stretch factor along the elongated direction.

Flight tests were conducted using a micro air vehicle platform (Fig. 3) developed at CU Boulder. The MAV consists of a foam RC kit augmented with an avionics package developed in house [3]. The avionics include GPS, pressure altitude, and a roll rate gyro as the only onboard sensors and wireless communication using an XBee Pro IEEE 802.15.4 (ZigBee) radio.

Fig. 3. Micro air vehicle flight control platform containing an avionics package with GPS, pressure and roll rate gyro plus XBee Pro ZigBee radio.

Figure 4 shows flight data of a MAV tracking a racetrack pattern. Blue arrows show the racetrack warped vector field direction, with vector length indicating the vector magnitude. The red line shows the zero level set of the warped vector field, i.e. the racetrack attractor for the vehicle motion. The black line shows the measured data from flight test of a UA, beginning at the plus sign with location near (-220,-140) m and a heading of approximately 150 degrees (measured CCW from the positive x-axis). Note

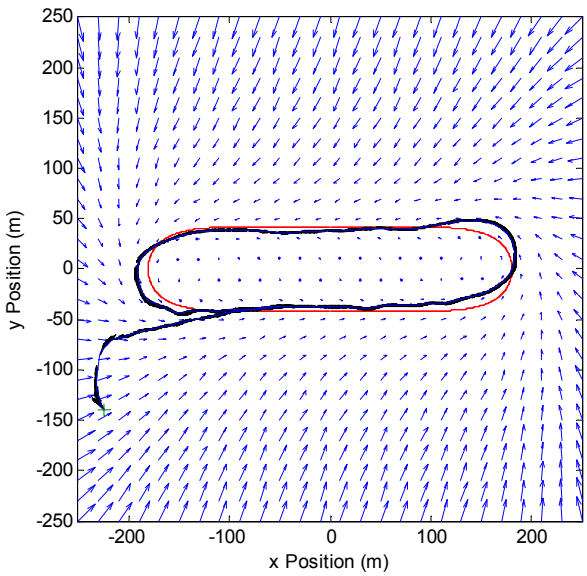

Fig. 4. Experimental results of a micro air vehicle tracking a circular loiter pattern warped into a racetrack.

the restricted turn rate on the vehicle causes poor vector field tracking initially, but once the initial heading error is corrected, the vehicle follows the vector field flow to track the race track path. Disturbances from wind and GPS errors prevent exact path tracking.

IV. Extremum Seeking for Electronic Chaining

Extremum seeking (ES) [8] controllers are adaptive, model free controllers designed to drive the set point of a dynamic system to an optimal, but unpredictable, location defined by a performance function that is only known to have an extremum point. In the ES framework, a sinusoidal dither signal is introduced onto the inputs into the plant to obtain a time varying sinusoidal output of the measurable performance metric as seen in Fig. 5. This sinusoidal output is then demodulated with another phase corrected sine wave to obtain a measure of the local gradient of the performance metric.

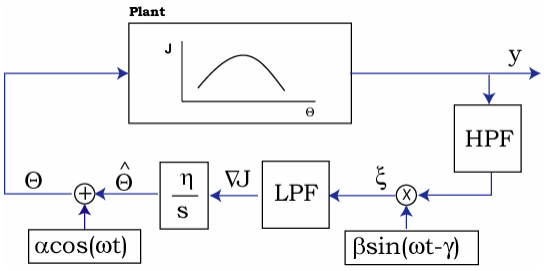

Fig. 5. Typical extremum seeking control algorithm.

From inspection of Fig. 5, one can see that the input into the plant can be expressed as

$$\theta = \alpha \cos(\omega t) + \hat{\theta} \tag{10}$$

where θ is the input into the plant, α is the dither signal

amplitude and ω is the dither frequency. In two dimensions, this equation has the structure of a circular perturbation about a moving center point $\hat{\theta}$. In [9] the authors took advantage of this similarity and designed a new ES algorithm (see Fig. 6) using a LGVF controller to control the motion of a nonholonomic vehicle acting as a communications repeater.

The most notable difference between the new ES algorithm and the typical approach is that instead of adding an artificial external dither signal to the local estimate and applying that to the plant inputs directly, the dither signal is provided by the physical (circular) motion of the vehicle that results from using a LGVF controller about an orbit point. The primary benefit of using the physical motion of the vehicle is that the resulting demodulation generates a true path gradient and thus does not require phase correction. However, the drawback is that the responsiveness (e.g. rate of convergence) of the system is limited by the performance constraints of the UA.

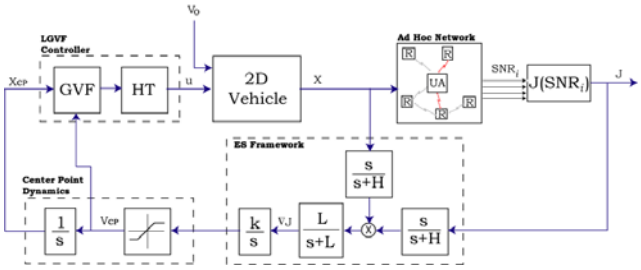

Fig. 6. An extremum seeking algorithm for a single vehicle in linked network chain of vehicles.

The ES controller presented in [9] (shown in Fig. 6) was designed to control the motion of an unmanned aircraft, acting as a communication repeater, by driving the location of the center point given to the LGVF controller to a point that provides optimal communication between two otherwise disconnected nodes. To obtain a location of optimal communication performance, the objective function for the ES algorithm was defined as

$$J(\mathbf{p}_j) = (1/S_{j,j-1} - 1/S_{j,j+1})^2 \qquad (11)$$

where $\boldsymbol{p}$ is the position of the UA and $S_{j,j-1}$, $S_{j,j+1}$ are the signal-to-noise ratios (SNR) as measured by UA j at location $\boldsymbol{p}$ for the two radios (j-1 and j+1) for which it is relaying traffic. This formulation results in a smooth positive definite function that has a minimum when the two SNRs are equal.

While there are empirical models [9] that relate signal strength to geographic distance, there are numerous factors such as antenna orientation and environmental interference noise that makes it almost impossible to predict this relationship in advance. To understand how the SNR field can differ from the empirical model, several different flight tests have been conducted using the *Ares* UA (Fig. 7) and the Ad-hoc UAS Ground Network (AUGNet) [6] developed at CU Boulder. These tests measured SNR as a function of the UA location between two similar 802.11b radios. A contour plot of the SNR field given off by a ground node as measured on board Ares during one of the tests is shown in Fig. 8. The figure shows the RSSI field using a one-watt amplifier on the ground and UA nodes, feeding to a simple quarter-wave whip antenna, during the first 10 minutes of flight. As expected, the shape of the field shows power dropping off with increasing distance, but also shows that the field will have irregularities that cannot be predicted.

Fig. 7. The CU Ares unmanned aircraft system.

Figure 9 plots the RSSI versus distance for the same dataset shown in Fig. 7 as measured by the UA and the ground node. In addition the best fit empirical model is also plotted with parameters of α=2.2 and K=5.01e7. From this plot it is easy to see the variability of the RSSI measurements with a UA, due in this case to the change in attitude of the antenna on the UA as the aircraft banks during turns. Even though Fig. 9 shows that the RSSI measurements can be fit to an empirical model, it is still difficult to predict the parameters for the model in dynamic environments.

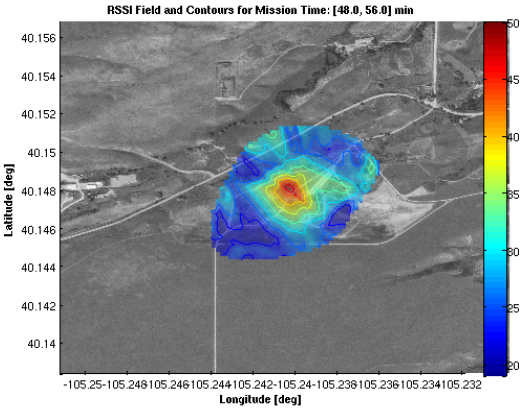

Fig. 8. Contour plot of RSSI measurements taken onboard Ares UA using 802.11b radios with 1W amplifier and whip antenna and overlaid over aerial photograph of flight range.

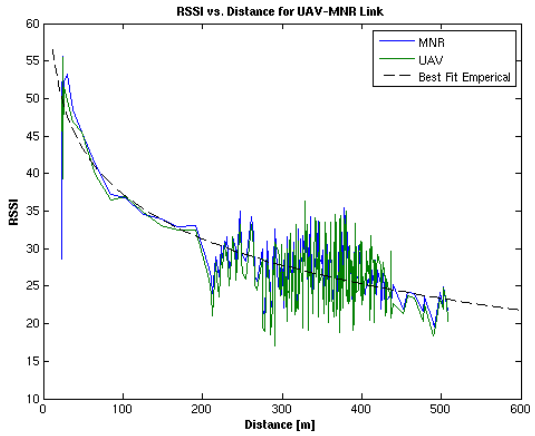

Fig. 9. Plot of RSSI measurements over distance for measurements made by both a UAV and a ground node shown in Fig. X1. Best fit model also shown with α=2.2 and K=5.01e7.

To conclude this section, Fig. 10 shows the results of a simulation of the Ares UA acting as a communication repeater using the ES algorithm based on the LGVF controller. The simulation was run with two static ground nodes (indicated as blue dots) with a localized noise source in the middle shown as the red diamond and the motion of the UA (in solid blue) tracking the center point (in slashed green). In the simulation, the motion of the UA is modeled to match the limited performance of the Ares UA. In addition, the radio parameters used in the simulation were based on the data shown in Fig. 8.

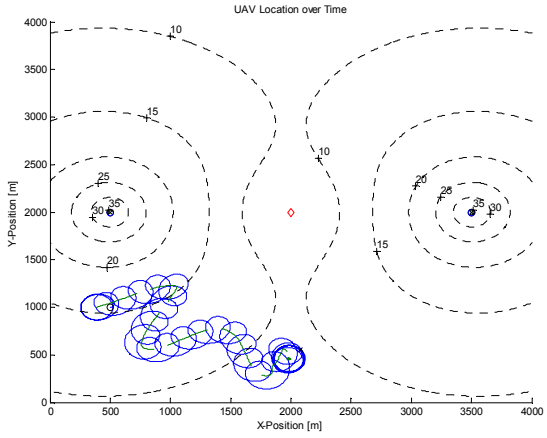

Fig. 10. Simulation of an unmanned aircraft in a network chain linking two static task nodes in the presence of a localized noise (indicated by a diamond). The orbit center point is shown as dashed red line with orbital motion of the UA shown in blue and the black dotted lines represent SNR level sets from the two task nodes.

V. Cooperative Tracking of Moving Targets

Cooperative stand-off line-of-sight (CSLOS) trajectories allow multiple UA to track moving ground targets while maintaining optimal sensor coverage and remaining outside a critical threat range (Fig. 11). Cooperation by multiple UA to track a single target improves geolocalization performance and decreases the target's ability to evade the team. Stand-off tracking reduces exposure of the UA to threats and allows them to conduct operations in a stealthy manner.

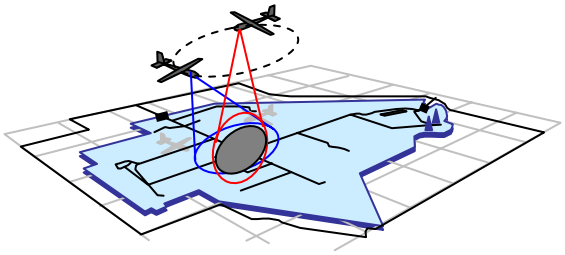

Fig. 11. Cooperative standoff line-of-sight tracking of a moving ground target by two cooperating unmanned aircraft.

CSLOS tracking of a moving target by two or more unmanned aircraft is achieved by coordinating the phase of the UA around the desired loiter pattern. Phase coordination is produced by adjusting the speed of the vehicles (within performance limits) and then processing them through the correction algorithm of Eq. (4) to maintain the desired standoff distance to the moving target. For two cooperating UA with phase angles θ_1 and θ_2 defined relative to the instantaneous target location and desired phase offset θ_D the phasing Lyapunov function V_p=(θ_2- θ_1- θ_D) is driven to zero with speed commands [1,2]

$$\begin{aligned} u_{1,1} &= k(\theta_2 - \theta_1 - \theta_D) r_d + v_0 \\ u_{1,2} &= -k(\theta_2 - \theta_1 - \theta_D) r_d + v_0 \end{aligned} \quad . \tag{12}$$

The CSLOS tracking algorithms are implemented in hardware-in-the-loop (HWIL) simulation using the Ad-hoc UAS Ground Network (AUGNet) and Networked UAS Communication, Command, and Control (NetUASC3) systems developed at CU Boulder [6, 7, 11]. An intelligent flight management system based on the CAN bus architecture connects vehicle subsystems to an ad-hoc wireless network for net-centric communication and cooperation between supervisory control elements onboard each vehicle [7, 11]. The supervisory controllers apply the CSLOS algorithms and send the speed and turn rate commands to a PiccoloPlus autopilot. No ground-based computation is performed or required for any of the scenarios.

Figure 12 shows HWIL simulation results of two UA tracking a static target with desired relative phasing of $\pi/2$ radians and a standoff radius of 300 meters. The top two plots show the latitude and longitude of each UA. The third plot shows the speed command for each vehicle and the fourth plot shows the turn rate command for each vehicle. The aircraft were started at nearly identical orbit phase, and the controller was started slightly after t=2.65 * 10^6 ms (identifiable by the jump in commanded airspeed of Ares 3). Each UA provided relative phase information

asynchronously to the other UA at a rate of 1 Hz. The affect of the controller on phasing of the UA is quite apparent in the position data.

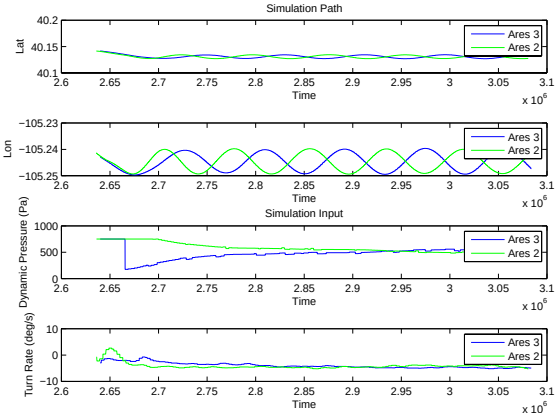

Fig. 12. Two UAs tracking a static target. a.)Latitude of each UA. b.) Longitude of each UA. c.) Speed command for each vehicle d.) Turn rate command for each vehicle all vs time (ms).

Figure 13 shows HWIL simulation results of two UA tracking a dynamic target that moves with velocity [0 m/s, 10 m/s]. The target was "released" at approximately 20.5 minutes ($1.23 * 10^6$ ms) into the flight, which coincides with the spike in commanded speed. Examining the plot, both UA enter into an orbit at the correct phasing and maintain it throughout the experiment. Evidence of the moving target can be seen in the oscillatory commanded airspeed (highest magnitude when the UA is traveling in the same direction as the target), and in the steady trend toward a lower latitude for both UAs over the flight.

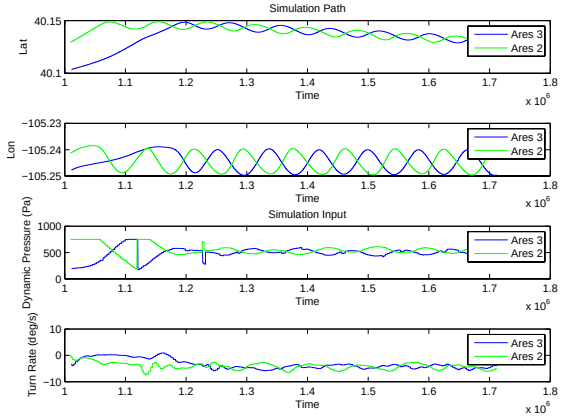

Fig. 13. Two UAs tracking a moving target. a.)Latitude of each UA. b.) Longitude of each UA. c.) Speed command for each vehicle d.) Turn rate command for each vehicle all vs time (ms).

VI. Conclusion

This paper presented the use of a guidance vector field method for different unmanned aircraft applications. These applications included low-level control in a hierarchical architecture for toxic plume tracking by micro air vehicles; controlled mobility in ad-hoc networks using extremum seeking to improve communication performance; and cooperative stand-off line-of-sight tracking of moving targets. In each case, the Lyapunov vector field algorithm provided a low-level, globally stable, loiter behavior that is used by higher levels in the control architecture. Simulation results and flight data from different platforms performing different applications verify the vector field approach.

References

[1] E. W. Frew, D. A. Lawrence and S. Morris, "Cooperative Standoff Line-of-Sight Tracking of Moving Targets using Modified Lyapunov Guidance Vector Fields," Submitted to *the AIAA Journal of Guidance, Control, and Dynamics,* 2006.

[2] E. W. Frew and D. Lawrence, "Cooperative stand-off tracking of moving targets by a team of autonomous aircraft," in *AIAA Guidance, Navigation, and Control Conference, San Francisco, CA,* 2005.

[3] W. Pisano, D. Lawrence, and K. Mohseni, "Concentration Gradient and Information Energy for Decentralized UAV Control", in *AIAA Guidance, Navigation, and Control Conference*, Keystone, CO, 2006.

[4] C. Dixon and E. W. Frew, "Controlling the Mobility of Network Nodes using Decentralized Extremum Seeking," to appear in *45th IEEE Conference on Decision and Control,* San Diego, CA, Dec. 2006.

[5] R. Rysdyk, C. Lum and J. Vagners, "Autonomous orbit coordination for two unmanned aerial vehicles," in *AIAA Guidance, Navigation, and Control Conference 2005, Aug 15-18 2005,* 2005, pp. 4876-4884.

[6] Brown, T. X., Argrow, B., Dixon, C., Doshi, S., Thekkekunnel, R.-G., and Henkel, D., "Ad Hoc UAV Ground Network (AUGNet)," Proc. AIAA 3rd Unmanned Unlimited Technical Conference, Workshop and Exhibit, Chicago, Illinois, Sept. 2004.

[7] J. Elston, E. W. Frew, and B. Argrow, "Networked UAV Command, Control and Communication," in AIAA Guidance, Navigation, and Control Conference, Keystone, CO, 2006.

[8] K. B. Ariyur and M. Krstic, *Real-Time Optimization by Extremum-Seeking Control.* Hoboken, NJ: John Wiley & Sons, Inc, 2003

[9] C. Dixon and E. W. Frew, "Controlling the mobility of network nodes using decentralized extremum seeking," accepted to *45th IEEE Conference on Decision and Control,* 2006, 11-12 December, San Diego, CA.

[10] D. A. Lawrence, E. W. Frew, and W. J. Pisano, ``Lyapunov vector fields for autonomous UAV flight control'', To appear, 2007 *AIAA Guidance, Navigation, and Control Conference,* Aug., 2007.

[11] Jack Elston and Eric W. Frew. "Net-centric Cooperative Tracking of Moving Targets". To appear *AIAA Infotech@Aerospace*, Rohnert Park, CA, May 2007.